Multiplicative versus Additive Bias Field Models for Unified Partial-Volume Segmentation and Inhomogeneity Correction in Brain MR Images

Su Wang, Lihong Li, Hongbing Lu and Zhengrong Liang

Abstract— **It has been widely accepted that for brain MR images, both the image density inhomogeneity (slowly-varying intensity changes across the field of view) and partial-volume effect (PVE) (more than one tissue type present in a single voxel) considerably reduce the accuracy and reliability of quantitative analysis for various clinical purposes. This paper presents a unified expectation-maximization (EM) approach, where PVE and intensity inhomogeneity are combined together into a built-in-one statistical model in additive and multiplicative formats. It assumes that each tissue type follows a conditionally-independent normal distribution, based on which the summation of all tissue contributions multiplied or added by the bias term leads to mean density value at each voxel. Meanwhile, the summation of all the tissue mixtures, which is unobservable but could be estimated via EM framework (many-to-one mapping), multiplied or added by the bias term would lead to the observed image density at each voxel. In doing so, both the inhomogeneity and tissue mixtures are updated voxel-by-voxel until the convergence of a stable solution. Comprehensive tests on simulated brain MR images strongly demonstrated the feasibilities of additive/multiplicative bias models and the effectiveness of the unified EM approach. In addition, additive and multiplicative bias field models reflect advantages in terms of stability and robustness.**

Index Terms— **MAP-EM algorithm, image segmentation, Inhomogeneity correction, partial volume effect**

I. Introduction

Magnetic resonance imaging (MRI) has received considerable attention as an advanced medical imaging technique for various clinical purposes due to its irreplaceable advantages over other imaging techniques in providing high-contrast images between soft tissues. Segmenting MR images for quantitative analysis of tissue characteristics has played a significant role in applying MRI for various clinical applications and has been remaining yet a research interest. However intensity inhomogeneity, which refers to the slowly-varying intensity changes across the field-of-view, violates the uniformity property of a single tissue statistical distribution, and therefore impedes the accuracy and reliability of image segmentation.

Efforts have been made to correct intensity non-uniformity by following two relatively independent tracks. One is to model, estimate and correct inhomogeneity priori to the image classification, and the most recent progress in this category can be summarized mainly into three categories, (1) low-frequency model -- intensity inhomogeneity occupies the low frequency domain and could be corrected by designing an adequate filter [1-3], (2) hypersurface model -- intensity inhomogeneity may be fitted by designing an adequate smoothing function/basis [4-6], and (3) statistical model -- intensity inhomongneity is assumed as a random process and could be estimated via Bayesian or maximum *a posteriori* (MAP) framework [7-8], *etc*. The other track is to combine image segmentation and inhomogeneity correction into a common framework, such that they could interact with each other and, therefore, be jointly estimated as a whole. As soft segmentation estimates tissue mixture fractions for continuous class labeling instead of assigning discrete and limited numbers [9-10], it is generally recognized that solving any of them could definitely benefit the other one because of their reciprocal characteristic. Ashburner *et al*. [11] proposed a unified statistical model, where inhomogeneity bias term was assumed to be associated with both tissue mean and variance and a tissue probability map was required for modeling the spatial bias field. However for optimization, a composite iteration strategy was taken, *i.e*., each iteration involved alternation between two separate algorithms of Expectation-Maximization (EM) and Levenberg-Marquardt (LM) to estimate tissue type parameters and bias field (BF) respectively. In this paper, an alternative unified framework is proposed with a convertible bias field model, where both tissue mixture fractions and BF were updated simultaneously via regularized EM iterations for a MAP solution. By assuming each tissue type as a conditionally-independent normal distribution, the summation of all tissue mixtures' contributions inside each voxel leads to the image density mean of that voxel, and the summation of all tissue mixtures' unobservable random processes leads to the observed image

This work was partly supported by NIH Grant #CA082402 and #CA120917 of the National Cancer Institute.

Su Wang is with the Department of Radiology, State University of New York, Stony Brook, NY 11794 USA (e-mail: suwang@mil.sunysb.edu).

Lihong Li is with the Department of Engineering Science and Physics, College of Staten Island, City University of New York, Staten Island, NY 10314, USA.

Hongbing Lu is with the Department of Computer application, Fourth Military Medical University Xi'an, Shaanxi 710032, China

Zhengrong Liang is with the Department of Radiology and Physics, State University of New York, Stony Brook, NY 11794 USA

density. Meanwhile, the presence of BF is assumed to affect image density means only, while keeping tissue variances unchanged. To ensure a smoothly-changing bias field, an extra regularization term involving the first- and second-order derivatives was included into the derived energy function.

The remainder of this paper is organized as follows. Section II presents a unified statistical framework of merging tissue mixture proportions and bias field together, where two alternatives of multiplicative and additive bias field models are described. Section III validates the utility of our proposed framework by conducting experiments on a digital MRI phantom with some conclusions drawn in Section IV.

II. A Unified Statistical Model for Segmentation and Inhomogeneity Correction

In this section, a unified statistical framework jointly estimating both tissue mixture proportions and bias field is presented by referring to our previous PV-based Gaussian mixture model [9-10].

A. Multiplicative vs. Additive Bias Models

Assume the image contains *K* tissue types, with μ_k and ν_k ($k = 1,2,\ldots,K$) be the uniformly-distributed intensity mean and variance of tissue type *k*. If we further define Z_{ik} ($\sum_{k=1}^{K} Z_{ik} = 1$, $0 \le Z_{ik} \le 1$) as the tissue mixture proportion of tissue type k partially filling in voxel *i* ($i = 1,2,\ldots,I$), and ρ_i is the bias term associated with voxel *i*, then a multiplicative bias field model reflecting the observed image voxel intensity Y_i ($i = 1,\ldots,I$) could be depicted as

$$Y_i = \rho_i \sum_{k=1}^{K} Z_{ik}\mu_k + n_i \tag{1}$$

where additive noise n_i follows a zero-mean Gaussian distribution with variance $\sum_{k=1}^{K} Z_{ik}\nu_k$.

Although the multiplicative bias field has been widely used by most of the existing tissue classification algorithms, an alternative additive model could be obtained by imposing bias field term onto tissue mean μ_k only, which becomes

$$Y_i = \sum_{k=1}^{K} Z_{ik}\mu_{ki} + n_i = \sum_{k=1}^{K} Z_{ik}(\beta_i + \mu_k) + n_i \tag{2}$$

where μ_{ki} is the altered local mean of tissue class *k* at voxel *i*. At the first glimpse, Eqs. (1) and (2) are conceptually different models, however given observation Y_i at current voxel *i,* we have

$$\begin{aligned} \rho_i \sum_{k=1}^{K} Z_{ik}\mu_k &= \sum_{k=1}^{K} Z_{ik}(\beta_i + \mu_k) \\ &= \sum_k Z_{ik}\beta_i + \sum_k Z_{ik}\mu_k \\ &= \beta_i + \sum_k Z_{ik}\mu_k \\ &= \left(\frac{\beta_i}{\sum_k Z_{ik}\mu_k} + 1\right)\sum_k Z_{ik}\mu_k \end{aligned} \tag{3}$$

where the relationship between two bias terms, ρ_i and β_i, have the following relationship

$$\rho_i = \left(\frac{\beta_i}{\sum_k Z_{ik}\mu_k} + 1\right). \tag{4}$$

The major difference between (1) and (2) is the different domains where ρ_i and β_i are located. For the example of 20% intensity non-uniformity, ρ_i falls into the scope of [0.9, 1.1] while β_i fluctuates heavily around zero with its sign determined by $(\rho_i - 1)$, and its magnitude largely depending upon $\sum_{k=1}^{K} Z_{ik}\mu_k$.

B. MAP-EM Algorithm for In-complete Data

B.1. Multiplicative Bias Field Model

Without loss of generality, we assume that the acquired image intensity Y_i at voxel *i* follow a normal distribution, given parameters $\{\mu_k \ \nu_k, Z_{ik}, \rho_i\}$ respectively

$$p(\mathbf{Y} \mid \{\mu_k\},\{\nu_k\},\{Z_{ik}\},\{\rho_i\}) = \prod_{i=1}^{I} \frac{1}{\sqrt{2\pi\sum_{k=1}^{K} Z_{ik}\nu_k}} \exp\left\{-\frac{\left(Y_i - \rho_i\sum_{k=1}^{K} Z_{ik}\mu_k\right)^2}{2\sum_{k=1}^{K} Z_{ik}\nu_k}\right\} \tag{5}$$

Directly estimating the tissue mixture proportions $\{Z_{ik}\}$, bias field $\{\rho_i\}$ and the tissue model parameters $\{\mu_k, \nu_k\}$ could be performed by maximizing the conditional probability distribution (5) with respect to each corresponding parameter. This would result in a set of nonlinear equations, whose solutions could be very challenging even if they are numerically tractable. Given the many-to-one mapping of observation Y_i at voxel *i* by different tissue classes, building a statistical model for estimating unobservable variables via the EM algorithm [12] is an alternative and effective solution. In the EM framework, the observation at each voxel *i* or Y_i is considered as an incomplete random variable, while the underlying contributions of each tissue type *k*, $\{X_{ik}, k = 1,2,...,K\}$, are considered as complete random variables reflecting the complete tissue mixture proportions and bias field information in each voxel. The probability distribution relationship between the incomplete data $\{Y_i\}$ and the complete data $\{X_{ik}\}$ is depicted by the following integral equation under the condition of (6)

$$P(Y_i \mid \{Z_{ik}\},\{\mu_k\},\{\nu_k\},\{\rho_i\}) = \int_{\{Y_i = \sum_{k=1}^{K} X_{ik}\}} P(X_{ik} \mid \{Z_{ik}\},\{\mu_k\},\{\nu_k\},\{\rho_i\})dX \tag{6}$$

and

$$p(\mathbf{X} \mid \{\mu_k\},\{\nu_k\},\{Z_{ik}\},\{\rho_i\}) = \prod_{i,k=1}^{I,K} \frac{1}{\sqrt{2\pi Z_{ik}\nu_k}} \exp\left\{-\frac{(X_{ik} - \rho_i Z_{ik}\mu_k)^2}{2Z_{ik}\nu_k}\right\} \tag{7}$$

where the integral is understood as the summation over all possible configurations of $\{X_{ik}, k = 1,2,...,K\}$, given Y_i. EM algorithm then seeks the solution of maximizing the expectation of conditional probability distribution (7) for complete-data. Alternatively, it tries to maximize the

expectation of the complete-data log likelihood utilizing the posterior distribution of the latent variables.

The conditional probability distribution (7) is basically a likelihood function given the tissue and model parameters. A maximum likelihood (ML) solution is usually not acceptable due to the presence of image noise. To overcome this dilemma, *a priori* constraints are intentionally imposed to ensure the continuity of the both underlying tissue mixture distribution as well as bias field continuity within the body for a penalized ML (pML) or MAP solution.

For the regularization term modeling tissue mixture distributions $\{Z_{ik}\}$, MRF model is employed by assuming that a voxel surrounded by one class, *e.g.*, non-brain tissue, cannot belong to other classes by imposing both spatial and anatomical constraints. In our study, an *a priori* penalty on Z_{ik} has the following general form of

$$P(Z_{ik} \mid \{Z_{ik\varepsilon_i}\}) = C^{-1} \times \exp\left[-\tfrac{1}{2}\alpha U(Z_{ik} - Z_{ik\varepsilon_i})\right] \tag{8}$$

where $\{Z_{ik\varepsilon_i}\}$ indicate the surrounding voxels' Z_{ik} in the neighboring system ε_i, C is a normalization constant and α is an adjustable parameter controlling the degree of the penalty. The energy function $U(.)$ can be written as a quadratic form of

$$U(Z_{ik}) = \sum_{r\in\varepsilon_i} w_{ir} \cdot (Z_{ik} - Z_{rk})^2, \tag{9}$$

where index r indicates the neighbors ε_i and w_{ir} is a weighing factor for different orders of the neighbors.

We follow the same way as Pham did in his study [13] to impose priori constraint on bias field $\{\rho_i\}$, where both first- and second-order regularization terms were used to ensure the spatial smoothness and slow variation of bias field $\{\rho_i\}$ across the field of view. Thus we have the following energy function

$$U(\rho_i) = \gamma_1 \sum_{j=1}^{R} \left(D_j * \boldsymbol{\rho}\right)_i^2 - \gamma_2 \sum_{j,k=1}^{R} \left(D_j * D_k * \boldsymbol{\rho}\right)_i^2 \tag{10}$$

where R equals 2 for two-dimensional (2D) slice images and 3 for 3D volume images. Vector $\boldsymbol{\rho}$ denotes the entire bias field, and notation D is the standard forward finite difference operator along the corresponding directions. Symbol * denotes the 1D discrete convolution operator. The first-order regularization term (associated with γ_1) penalizes a large variation in the bias field and the second-order regularization term (associated with γ_2) penalizes the discontinuities in the bias field, both of which significantly control the degree of smoothness of the bias field.

Given equations (1)-(10), an EM approach to MAP solution of jointly estimating the tissue model parameters $\{\mu_k, \nu_k\}$, tissue mixture proportions $\{Z_{ik}\}$, as well as bias field $\{\rho_i\}$ is presented below.

Initialization: As the very first step of EM algorithm, initialize $\{\mu_k, \nu_k\}$, $\{Z_{ik}\}$ and $\{\rho_i\}$ as $\{\mu_k^{(0)}, \nu_k^{(0)}\}$, $\{Z_{ik}^{(0)}\}$ and $\{\rho_i^{(0)}\}$.

(2) *E-step*: This step computes the conditional expectation of the complete-data likelihood (7) penalized by MRF-modeled tissue component distribution $p(\mathbf{Z})$ and regularized bias priori $p(\boldsymbol{\rho})$, given the acquired data $\{Y_i\}$ and current parameter estimation $\Theta^{(n)}$, which is

$$\begin{aligned} Q(\Theta \mid \Theta^{(n)}) &= \mathrm{E}_{Y=\Sigma_k X_{ik}}\left[\ln\left(p(\mathbf{X}\mid\Theta)\cdot p(\mathbf{Z})\cdot p(\boldsymbol{\rho})\right) \mid \mathbf{Y}, \Theta^{(n)}\right] \\ &= \mathrm{E}_{Y=\Sigma_k X_{ik}}\left[-\frac{1}{2}\sum_i\sum_k\left\{\ln(2\pi)+\ln(Z_{ik}\nu_k)+\frac{1}{Z_{ik}\nu_k}\left[X_{ik}^2 - 2\rho_i Z_{ik}\nu_k X_{ik} + \rho_i^2 Z_{ik}^2 \nu_k^2\right]\right.\right. \\ &\quad \left.\left. + 2\alpha\sum_{r\in\varepsilon_i} w_{ir}(Z_{ik}-Z_{rk})^2 + 2\left(\gamma_1\sum_{j=1}^{R}(D_j*\rho)_i^2 + \gamma_2\sum_{j,l=1}^{R}(D_j*D_l*\rho)_i^2\right)\right\} \middle| Y_i, \Theta^{(n)}\right] \end{aligned} \tag{11}$$

By the use of preceding conditional expectations, conditional expectation X_{ik} and X_{ik}^2 in (11) are simplified as

$$\begin{aligned} X_{ik}^{(n)} &= \mathrm{E}_{Y=\Sigma_k X_{ik}}\left[X_{ik} \mid Y_i, \Theta^{(n)}\right] = \rho_i^{(n)} Z_{ik}^{(n)} \mu_k^{(n)} + \frac{\left(Z_{ik}^{(n)}\nu_k^{(n)}\right)}{\sum_{j=1}^{K} Z_{ij}^{(n)}\nu_j^{(n)}}\left(Y_i - \rho_i^{(n)}\sum_{j=1}^{K} Z_{ij}^{(n)}\mu_j^{(n)}\right) \\ (X_{ik}^2)^{(n)} &= \mathrm{E}_{Y=\Sigma_k X_{ik}}\left[X_{ik}^2 \mid Y_i, \Theta^{(n)}\right] = \left(X_{ik}^{(n)}\right)^2 + \left(Z_{ik}^{(n)}\nu_k^{(n)}\right)\frac{\sum_{j\neq k}^{K}\left(Z_{ij}^{(n)}\nu_j^{(n)}\right)}{\sum_{j=1}^{K}\left(Z_{ij}^{(n)}\nu_j^{(n)}\right)} \end{aligned} \tag{12}$$

(3) *M-step*: This step maximizes the conditional expectation of (11) for the (n+1)-th iterated estimate of the tissue model parameters, mixture percentages and bias field by simply setting the partial derivatives of $Q(\Theta \mid \Theta^{(n)})$ with respect to μ_k, ν_k, Z_{ik} and ρ_i to zero respectively.

For parameters μ_k and ν_k, we have

$$\frac{\partial Q}{\partial \mu_k}\Big|_{\mu=\mu^{(n+1)}} = 0 \quad \Rightarrow \quad \mu_k^{(n+1)} = \frac{\sum_i \rho_i^{(n)} X_{ik}^{(n)}}{\sum_i \left(\rho_i^2\right)^{(n)} Z_{ik}}. \tag{13}$$

$$\nu_k^{(n+1)} = \frac{1}{I}\sum_i \frac{(X_{ik}^2)^{(n)} - 2\rho_i^{(n)} X_{ik}^{(n)} Z_{ik}^{(n)} \mu_k^{(n)} + (\rho_i^2 Z_{ik}^2 \mu_k^2)^{(n)}}{Z_{ik}^{(n)}}. \tag{14}$$

Taking partial derivative of (11) with respective to Z_{ik} leads to a nonlinear equation up to fifth-order with dramatically increasing numerical complexity. In practice, the conditional expectation (11) can be approximated as a quadratic term by fixing $\sigma_{ik}^2 = Z_{ik}\nu_k$ in the numerator of (11) as a priori from the current-iterated results to the next iteration. Therefore we have Eqs. (15)-(17) for the cases of two and three tissue classes respectively

$$Z_{i1}^{(n+1)} = \frac{X_{i1}^{(n)}(\sigma_{i2}^2)^{(n)}\mu_1^{(n)}\rho_i^{(n)} + (\mu_2^2)^{(n)}(\sigma_{i1}^2)^{(n)}\rho_i^{(n)} - X_{i2}^{(n)}(\sigma_{i1}^2)^{(n)}\mu_2^{(n)}\rho_i^{(n)} + 4\alpha(\sigma_{i1}^2)^{(n)}(\sigma_{i2}^2)^{(n)}\sum w_{ir} Z_{r1}^{(n)}}{(\mu_1^2)^{(n)}(\sigma_{i2}^2)^{(n)}\left(\rho_i^2\right)^{(n)} + (\mu_2^2)^{(n)}(\sigma_{i1}^2)^{(n)}\left(\rho_i^2\right)^{(n)} + 4\alpha(\sigma_{i1}^2)^{(n)}(\sigma_{i2}^2)^{(n)}\sum w_{ir}}. \tag{15}$$

(1)

$$\begin{cases} Z_{i1}+Z_{i2}+Z_{i3}=1 \\ Z_{i1}(U_0-U_1)+Z_{i2}(U_3-U_4)+Z_{i3}(U_6-U_7)=b_0-b_1 \\ Z_{i1}(U_0-U_2)+Z_{i2}(U_3-U_5)+Z_{i3}(U_6-U_8)=b_0-b_2 \end{cases} \quad (16)$$

where

$$U_0=\frac{(\mu_1^2)^{(n)}\left(\rho_i^2\right)^{(n)}}{(Z_{i1}\nu_1)^{(n)}}+2\alpha\sum_r w_{ir},\ U_1=U_2=U_3=0,$$

$$U_4=\frac{(\mu_2^2)^{(n)}\left(\rho_i^2\right)^{(n)}}{(Z_{i2}\nu_2)^{(n)}}+2\alpha\sum_r w_{ir},\ U_5=U_6=U_7=0$$

$$U_8=\frac{(\mu_3^2)^{(n)}\left(\rho_i^2\right)^{(n)}}{(Z_{i3}\nu_3)^{(n)}}+2\alpha\sum_r w_{ir},$$

$$b_0=\frac{X_{i1}^{(n)}\mu_1^{(n)}\rho_i^{(n)}}{(Z_{i1}\nu_1)^{(n)}}+2\alpha\sum_r w_{ir}Z_{r1}^{(n)},$$

$$b_1=\frac{X_{i2}^{(n)}\mu_2^{(n)}\rho_i^{(n)}}{(Z_{i2}\nu_2)^{(n)}}+2\alpha\sum_r w_{ir}Z_{r2}^{(n)},$$

$$b_2=\frac{X_{i3}^{(n)}\mu_3^{(n)}\rho_i^{(n)}}{(Z_{i3}\nu_3)^{(n)}}+2\alpha\sum_r w_{ir}Z_{r3}^{(n)}. \quad (17)$$

Finally, we have (18) for estimating the bias field $\{\rho_i\}$

$$\sum_{k=1}^{K}\frac{\mu_k^{(n)}X_{ik}^{(n)}}{\nu_k^{(n)}}=\rho_i^{(n)}\sum_{k=1}^{K}\frac{\mu_k^{2(n)}Z_{ik}^{(n)}}{\nu_k^{(n)}}+2\gamma_1\left(H_1*\rho\right)_i+2\gamma_2\left(H_2*\rho\right)_i \quad (18)$$

As suggested in [13], H_1 and H_2 are defined as

$$H_1=\begin{bmatrix}0&-1&0\\-1&4&-1\\0&-1&0\end{bmatrix},\ H_2=\begin{bmatrix}0&0&1&0&0\\0&2&-8&2&0\\1&-8&20&-8&1\\0&2&-8&2&0\\0&0&1&0&0\end{bmatrix} \quad (19)$$

B.2. Additive Bias Field Model

So far, we have fully described the mathematical derivations of the proposed MAP-EM solutions for jointly estimating tissue mixture proportions $\{Z_{ik}\}$ and bias field $\{\rho_i\}$ based on a multiplicative bias model. As such, an alternative additive model could be easily derived by replacing $\rho_i\mu_k$ with $\beta_i+\mu_k$, wherever it occurs. To preserve the presentation simplicity, the intermediate process is omitted and only the final derivations of $\{\mu_k^{(n+1)},\nu_k^{(n+1)}\}$, $\{Z_{ik}^{(n+1)}\}$ and $\{\beta_i^{(n+1)}\}$ are presented as (20-22).

$$\mu_k^{(n+1)}=\frac{\sum_i\left(X_{ik}^{(n)}-\beta_i^{(n)}Z_{ik}^{(n)}\right)}{\sum_i Z_{ik}} \quad (20)$$

$$\nu_k^{(n+1)}=\frac{1}{I}\sum_i\frac{(X_{ik}^2)^{(n)}-2X_{ik}^{(n)}Z_{ik}^{(n)}\left(\mu_k^{(n)}+\beta_i^{(n)}\right)+Z_{ik}^{2(n)}\left(\mu_k^{(n)}+\beta_i^{(n)}\right)^2}{Z_{ik}^{(n)}} \quad (21)$$

Simply by converting the multiplicative terms of $\mu_k\rho_i$ into $\mu_k+\rho_i$, and $\mu_k^2\rho_i^2$ into $(\mu_k+\rho_i)^2$ in (15-17), we got the derivations of $\{Z_{ik}\}$ corresponding to K=2 and 3 respectively, which are omitted here for presentation simplicity. Finally, for additive bias field estimation, we get

$$\sum_{k=1}^{K}\frac{X_{ik}^{(n)}-Z_{ik}^{(n)}\mu_k^{(n)}}{\nu_k^{(n)}}=\beta_i^{(n)}\sum_{k=1}^{K}\frac{Z_{ik}^{(n)}}{\nu_k^{(n)}}+2\gamma_1\left(H_1*\boldsymbol{\beta}\right)_i+2\gamma_2\left(H_2*\boldsymbol{\beta}\right)_i \quad (22)$$

III. Digital Brain MRI Phantom Study

The digital brain phantoms obtained from McConnell Brain Imaging Center of the Montreal Neurological Institute were used to evaluate our method [14]. For this study, we downloaded the 3D T1 phantom images with adjustable noise and inhomogeneity levels.

A. Brain MRI Phantom Simulation

The available 3D T1 phantom images could be well-adapted to our study by taking the following preparison steps, such that additive Gaussian noise with adjustable variance as well as 20% inhomogeneity was produced.

(1) Apply the provided simulator to generate a noise-free and uniform MRI brain phantom.

(2) Given the provided ground truth of $\{Z_{ik}\}$, voxels corresponding to 100% WM, GM and CSF are extracted for the purpose of computing tissue class mean $\{\mu_k\}$.

(3) Given user-defined tissue class variance $\{\nu_k\}$, calculated tissue class means $\{\mu_k\}$, provided tissue mixture proportions $\{Z_{ik}\}$ and priori distribution of bias field $\{\rho_i\}$ for voxel *i*, a brain MRI phantom with 20% inhomogeneity effect based on the multiplicative bias model could be generated by adding three gaussian-distributed random variables together, $N(\rho_i Z_{i1}\mu_1, Z_{i1}\nu_1)$, $N(\rho_i Z_{i2}\mu_2, Z_{i2}\nu_2)$, $N(\rho_i Z_{i3}\mu_3, Z_{i3}\nu_3)$ respectively, where $\{\rho_i\}$ has been rescaled to the domain of [0.9, 1.1]. Accordingly, an alternative additive bias model is straightforward by replacing $\rho_i\mu_k$ with $\beta_i+\mu_k$. Please be noted that the distribution of $\{\beta_i\}$ are calculated via $\{\rho_i\}$ by Eq. (4) for any associated quantitative analysis.

Figure 1 (a) illustrated a simulated brain MRI phantom of size 181×217×181 on the 83rd slice, with ground truths of $\{Z_{ik}\}$ and $\{\rho_i\}$ shown in (b-e) individually.

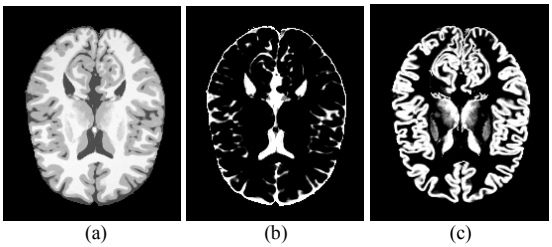

(a) (b) (c)

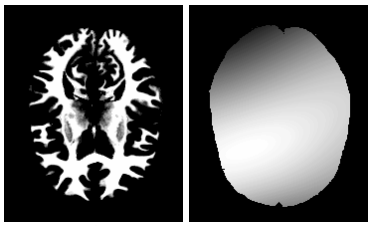

(d) (e)

Figure 1. Simulated brain MRI phantom on the 83rd slice, (a) digital image phantom with noise and 20% inhomogeneity effect, (b) ground truth of tissue mixture proportion $\{Z_{i1}\}$ corresponding to CSF, (c) ground truth of tissue mixture proportion $\{Z_{i2}\}$ corresponding to GM, (d) ground truth of tissue mixture proportion $\{Z_{i3}\}$ corresponding to WM, and (d) ground truth of bias field $\{\rho_i\}$.

B. Testing Results

In our previous study [10], we have discussed the sensitivity of EM algorithm to the initialization, *i.e.*, well initialized parameters would probably lead to global optima as well as fast convergence. For initializing $\{Z_{ik}^{(0)}\}$, we adopted the simplest way to randomize $\{Z_{ik}^{(0)}\}$ for each voxel, compared against the perfect way to set $\{Z_{ik}^{(0)}\}$ true to the ground. Things become much easier when we try to initialize $\{\rho_i^{(0)}\}$, either directly coming from the ground truth or simply setting $\{\rho_i^{(0)}\}$ to be zeros and ones for additive and multiplicative bias field models respectively.

Since the main focus of this paper is to investigate the interplay between $\{Z_{ik}\}$ and $\{\rho_i\}$ during EM iterations, the testing results are going to be presented by comparing three cases, (1) estimating $\{\rho_i\}$ only, (2) estimating $\{Z_{ik}\}$ only, (3) jointly estimating $\{Z_{ik}\}$ and $\{\rho_i\}$.

B.1. Estimating $\{\rho_i\}$ Only

Starting from the simplest case to test the validities of additive and multiplicative bias field models, only $\{\rho_i\}$ is updated during each EM iteration while keeping $\{Z_{ik}\}$ to its ground truth. After 100 iterations, we obtained the following estimated bias fields in Figure 2 corresponding to two different initialization schemes depending upon different bias field models.

For the purpose of quantitative analysis, each obtained $\{\rho_i\}$ was compared against the ground truth and the error rates defined as the averaged absolute value of the difference are plotted in Figure 3 versus EM iterations and initialization strategies. According to Figure 3, additive bias model has much faster converging speed compared to multiplicative model. However, we also found that such fast converging speed scarifies the stability of the estimated $\{\rho_i\}$. In other words, extra normalization step is required by additive bias field model to maintain the consistency between two consecutive EM iterations.

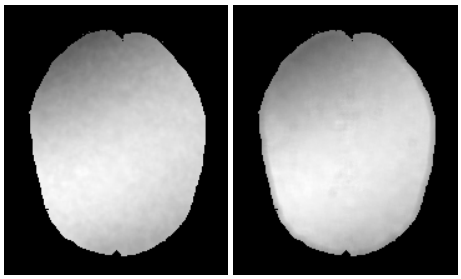

(a) (b)

Figure 2. Estimating $\{\rho_i\}$ only during each EM iteration corresponding to two different initialization schemes, (a) $\{\rho_i^{(0)}\}$ takes ones for multiplicative models, and (b) $\{\rho_i^{(0)}\}$ takes zeros for additive models.

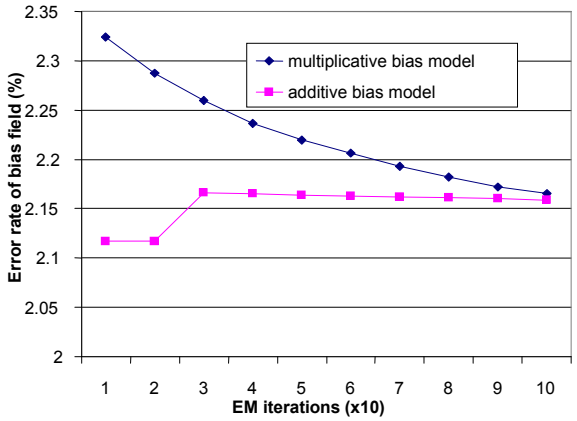

Figure 3. Plots of bias field error rate compared against ground truth versus EM iterations.

In summary, we would like to discuss a little bit about the values of γ_1, γ_2 that we chose for penalizing the first- and second-order derivatives of the bias field. We noticed that for multiplicative bias field model which has been widely accepted by many researchers that extremely large value of 40000 is required [13]. In our study, γ_1, γ_2 were equivalently set to be 20000. However, for the case of additive bias field model, pretty small values of γ_1, γ_2 of 0.00001 could meet our goal.

B.2. Estimating $\{Z_{ik}\}$ Only

Although in some cases, the ignorance of bias field $\{\rho_i\}$ could not result in significant visual distortion, the estimation of $\{Z_{ik}\}$ for quantitative analysis could be impaired to certain degrees. In this part, only $\{Z_{ik}\}$ is to be updated via EM iterations however fixing $\{\rho_i\}$ to ones or zeros depending upon different bias models to illustrate how $\{\rho_i\}$ affects the estimation accuracy of $\{Z_{ik}\}$. Following the same definition of error rate in Section B.1, Table 1 and Table 2 listed error rates corresponding to three tissue types for multiplicative and additive bias models respectively. Subject to the constraint

of $\sum_K Z_{ik} = 1$, the degree of freedom is actually (K-1). Thereafter, we are going to evaluate the error rates of $\{Z_{i1}\}$ and $\{Z_{i3}\}$ only corresponding to CSF and white matter respectively.

Table 1. Error rates of $\{Z_{ik}\}$ compared to ground truth when ignoring the presence of $\{\rho_i\}$ for multiplicative bias field model.

	Given accurate $\{\rho_i\}$	Ignore $\{\rho_i\}$
Error rate of CSF	1.798%	2.177%
Error rate of WM	5.983%	7.296%

Table 2. Error rates of $\{ Z_{ik} \}$ compared to ground truth when ignoring the presence of $\{\rho_i\}$ for additive bias field model.

	Given accurate $\{\rho_i\}$	Ignore $\{\rho_i\}$
Error rate of CSF	2.101%	2.183%
Error rate of WM	6.588%	7.388%

Shown in Table 1 and Table 2, it appears that the error rates of tissue mixture fractions were reduced when considering the presence of bias field $\{\rho_i\}$, with the maximum improvement ratios as high as 18% and 10% for multiplicative and additive bias models respectively.

B.3. Jointly Estimating $\{ Z_{ik} \}$ and $\{\rho_i\}$

Finally, $\{Z_{ik}\}$ and $\{\rho_i\}$ are going to be jointly estimated via every EM iteration in such a way that one of them updated itself by taking the already updated values of the other one. In sprite of its unified and general configuration of incorporating $\{Z_{ik}\}$ and $\{\rho_i\}$ together, it has its own drawback. EM iterations acted positively in some good conditions that $\{Z_{ik}\}$ and $\{\rho_i\}$ benefit each other to reach a balanced optima. However in other cases, they could also deteriorate each other, and even worse such deterioration could be accumulated and amplified resulting in the final noticeable deviations. Our testing results showed that compared to $\{Z_{ik}\}$, the estimation of $\{\rho_i\}$ is proven to be more sensitive to such accumulated distortion. Fortunately, such dilemma could be released a little bit by selecting good initializations. In what follows, table 3 listed the error rates of $\{Z_{ik}\}$ corresponding to CSF and white matter when applying both multiplicative and additive bias field models, where $\{Z_{ik}^{(0)}\}$ is randomly initialized and $\{\rho_i^{(0)}\}$ are set as ones or zeros for multiplicative and additive models respectively.

Table 3. Error rates of $\{Z_{ik}\}$ corresponding to three tissue classes when applying both multiplicative and additive bias field models.

	Multiplicative model	Additive model
Error rate of CSF	1.865%	2.166%
Error rate of WM	6.229%	7.319%
Error rate of $\{\rho_i\}$	1.063%	3.825%

And the estimated bias fields are shown in Figure 4 (a-b) as follows.

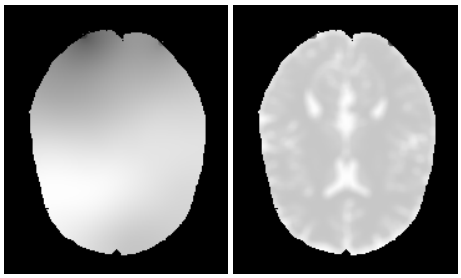

(a) (b)

Figure 4. Estimated bias fields from both multiplicative and additive models, (a) multiplicative model and (b) additive model

We found that for additive bias model, the smoothness of bias field $\{\rho_i\}$ as penalized by first- and second-order derivatives were impaired even though the error rates of $\{Z_{ik}\}$ have been reduced compared to those obtained by complete ignorance of $\{\rho_i\}$. We believe that such deterioration is caused by two factors, one is the interleaved iteration where error rate of $\{\rho_i\}$ is accumulated. More specifically, the smoothness of the $\{\rho_i\}$ in additive model largely depends upon the local variations of $\sum_k Z_{ik}\mu_k$, as shown in Eq. (3). The other factor is the fixed values of γ_1, γ_2 which would be otherwise adaptive to each iteration. However for multiplicative bias model, the smoothness of $\{\rho_i\}$ has been considerably preserved.

B.4. Comparison between Multiplicative and Additive Models

As a concluding remark and re-emphasizing Section III, we would like to fully summarize two models, multiplicative versus additive bias terms based on our comprehensive simulation results.

(1) No matter which bias model is considered, multiplicative or additive, the unified EM framework aims to jointly estimate $\{Z_{ik}\}$ and $\{\rho_i\}$ by merging these two together into one statistical model, i.e., updating any one of them involves the full knowledge of the other. Moreover, the greatest advantage of additive bias field model is its capability of maximally separating $\{Z_{ik}\}$ and $\{ \rho_i \}$ apart by the use of constraint $\sum_k Z_{ik} = 1$, as implied by Eq. (2). As such, when taking partial derivative of the energy function with respect to individual ρ_i and Z_{ik}, the obtained formulas become neat and much simpler compared against the multiplicative model, accompanied by the much faster converging speed as demonstrated by Figure 3.

(2) In terms of stability, we would like to point out that for additive bias field model, $\{\rho_i\}$ is directly imposed on tissue class mean and after derivations, it is found to be

closely tied to the additive noise term as in Eq. (2). In doing so, additive model turns out to be sensitive to the local observation Y_i and smoothness could be accordingly damaged by the term of $\sum_k Z_{ik}\mu_k$. Compared to more stable multiplicative model, an extra step of normalization to refine $\{\rho_i\}$ is taken after EM iterations to ensure the consistency between two consecutive iterations.

(3) The initialization schemes corresponding to different bias field models fully reflected the flexibility of multiplicative model once more. For quantitative analysis, the ground truth of $\{\rho_i\}$ is frequently encountered in the format of multiplicative term in the range of [0.9, 1.1] for 20% inhomogeneity effect. However, for converting multiplicative model to the case of additive model, Eq. (4) is suggested involving the full knowledge of $\{Z_{ik}\}$ as well as $\{\mu_k\}$ for all present tissue classes, which significantly limits the wide acceptance of additive bias model and therefore reduces its flexibility.

(4) Finally in terms of estimation accuracy and the gain by such unified MAP-EM statistics model, multiplicative bias model outperformed additive version. On one hand, the gain of $\{Z_{ik}\}$ when considering multiplicative bias model is almost 20% with less error in estimating $\{\rho_i\}$, as opposed to 10% gain of $\{Z_{ik}\}$ and higher $\{\rho_i\}$ estimation error when additive bias is concerned. On the other hand, the estimated $\{\rho_i\}$ via multiplicative model is guaranteed to be smoothly varying across the FOV, while additive bias model suffers from local variations of $\sum_k Z_{ik}\mu_k$, such that it is much inferior in the smoothness of $\{\rho_i\}$.

IV. CONCLUSION

In this paper, we present a unified MAP-EM framework to jointly estimate both bias field $\{\rho_i\}$ as well as tissue mixture proportions $\{Z_{ik}\}$ voxel by voxel, where two associated bias models are suggested for different purposes, multiplicative and additive cases. By imposing two penalty terms based on first-/second-order derivatives and MRF regularizing $\{\rho_i\}$ and $\{Z_{ik}\}$ respectively, each EM iteration jointly updates $\{\rho_i\}$ and $\{Z_{ik}\}$ parallelly maintaining their active interactions.

Gain has been observed by the fact that the estimation accuracy of $\{Z_{ik}\}$ has been improved compared against the case of complete ignorance of $\{\rho_i\}$, which is considered to be the major contributions of this paper. In addition, it is also found out that both multiplicative and additive bias models have their own advantages and disadvantages in terms of converging speed, sensitivity, stability as well as computational complexity.

It is worthwhile to point out that our additive bias model-based unified MAP-EM framework still suffer from a major problem, that is how to preserve the smoothness of bias field as iterations proceed. Although adaptive parameters are potentially helpful, efforts are suggested to seek for much stronger and controllable regularization term on preserving the smoothness of bias field, which would become our future work in this topic.

REFERENCES

[1] P. A. Narayana and A. Borthakur, "Effect of radio frequency inhomogeneity correction on the reproducibility of intracranial volumes using MRI image data," *Magnetic Resonance in Medicine*, vol. 33, no. 3, pp. 396-400, 1995.

[2] P. Irarrazabal, C. H. Meyer, D. G. Nishimura, and A. Macovski, "Inhomogeneity correction using an estimated linear field map," *Magnetic Resonance in Medicine*, vol. 35, no. 2, pp. 278-282, 1996.

[3] M. S. Cohen, R. M. Dubois, and M. M. Zeineh, "Rapid and effective correction of RF inhomogeneity for high field magnetic resonance imaging," *Human Brain Mapping*, vol. 10, no. 4, pp. 204-211, 2000.

[4] C. R. Meyer, P. H. Bland, and J. Pipe, "Retrospective correction of intensity inhomogeneities in MRI," *IEEE Transactions on Medical Imaging*, vol. 14, no. 1, pp. 36-41, 1995.

[5] J. Ashburner and K. J. Friston, "Voxel-based morphometry: the methods," NeuroImage, vol. 11, no. 6, part I, pp. 805-821, 2000.

[6] A. W. –C. Liew and H. Yan, "An adaptive spatial fuzzy clustering algorithm for 3-D MR image segmentation," *IEEE Transactions on Medical Imaging*, vol. 22, no. 9, pp. 1063-1075, 2003.

[7] R. Guillemaud and M. Brady, "Estimating the bias field of MR images," IEEE Transactions on Medical Imaging, vol. 16, no. 3, pp. 238-251, 1997.

[8] K. Held, E. R. Kops, B. J. Krause, W. M. Wells III, R. Kikinis, and H. M. Gartner, "Markov random field segmentation of brain MR images," IEEE Transactions on Medical Imaging, vol. 16, no. 6, pp. 878-886, 1997.

[9] S. Wang, H. Lu and Z. Liang, "A Theoretical Solution to Partial Volume MAP-EM Tissue Mixture Segmentation for CT/MRI Imaging Modalities," *International Workshop on Combinatorial Image Analysis, Buffalo, April 7-9, 2008.*

[10] D. Eremina, X. Li, W. Zhu, J. Wang, and Z. Liang, "Investigation on an EM framework for partial volume image segmentation," *Proceeding of SPIE on Medical Imaging*, vol. 6144, 2006.

[11] J. Ashburner and K. J. Friston, "A unified segmentation," *NeuroImage*, vol. 26, no. 3. pp. 839-851, 2002].

[12] A. Dempster, N. Laird, and D. Rubin, "Maximum likelihood from incomplete data via the EM algorithm," *Journal of the Royal Statistics Society*, vol. 39(B), pp. 1-38, 1977.

[13] D. Pham and J. Prince, "Adaptive fuzzy segmentation of magnetic resonance images", *IEEE Transactions on Medical Imaging*, vol. 18, no. 9, pp. 737-752, 1999.

[14] http://www.bic.mni.mcgill.ca/brainweb/